COBEM 2023 27TH INTERNATIONAL CONGRESS OF MECHANICAL ENGENEERING

ABCM Brazilian Society of Mechanical Sciences and Engineering
27th ABCM International Congress of Mechanical Engineering
December 04-08, 2023, Florianópolis-SC, Brazil

COB-2023-0057
STRUCTURAL OPTIMIZATION FOR RESONANCE-FREE TURBOMACHINERY BLISKS

Diego Zilli Lima
Daniel Jonas Dezan
Wallace Gusmão Ferreira
Federal University of ABC
Av. dos Estados, 5001 - Bangú, 09210-580, Santo André/SP, Brazil
diego.zilli@ufabc.edu.br
daniel.dezan@ufabc.edu.br
wallace.ferreira@ufabc.edu.br

Elóy Esteves Gasparin
Vitor Cesar Nogueira Mattos
Leandro Oliveira Salviano
UNESP – Ilha Solteira
Av. Brasil Sul, 56 – Centro, 15385-000, Ilha Solteira/SP, Brazil
eloy.gasparin@unesp.br
vitor.mattos@unesp.br
leandro.salviano@unesp.br

Jurandir Itizo Yanagihara
Escola Politécnica - University of São Paulo
Av. Prof. Mello Moraes, 2231 - Cidade Universitária, 05508-080, São Paulo/SP, Brazil
jiy@usp.br

Abstract. *The majority of turbomachinery failures are caused by fatigue, which is extremely sensitive to vibrations induced by operations in resonance regions. Because the efficiency of turbomachinery is intimately linked to its fluid and thermodynamic characteristics, most of the studies available in the literature focus on aerodynamic design only. Despite the benefits of structural design, such as lower mass, power, maintenance, material costs, and longer service life, there are fewer works of this genre available. Given the goal of creating the most efficient machine possible, minimizing the possibility of failures is fundamental; consequently, the work aimed to develop a structural optimization process of integrated bladed disks (blisks) focused on obtaining structures free of resonance, or having a lower risk of occurrence. A design technique for identifying possible resonance occurrences was applied to construct a resonance-free structure, in addition to mechanical design criteria for high-speed rotating blisks. Pre-stressed modal analysis was employed as the main method, which considered centrifugal loads, structural stiffening, spin-softening, and gyroscopic effects. The Campbell Diagram and other resonance identification methods were used to create the objective functions used in the optimization. The optimization strategy was a parametric optimization process based on metamodeling, also known as surrogate or response surface modeling. Case studies were used to validate the performance of the methodology. In all of them, the risk of resonance was reduced or even eliminated. Furthermore, structural integrity was improved as stress levels were also reduced.*

Keywords: *surrogate model, optimization, Campbell diagram, centrifugal compressor, resonance avoidance*

1. INTRODUCTION

This study is part of a larger project dedicated to the development of a supercritical CO2 (sCO2) centrifugal compressor train designed for application in a Carbon Capture, Storage, and Utilization (CCSU) plant. CCSU technologies encompass a range of approaches aimed at mitigating climate change by reducing CO2 emissions from various sources (Baena-Moreno *et al*., 2018; Bui *et al*., 2018). However, it is worth noting that certain aspects of these technologies, particularly large-scale deployment, and associated costs, are still under active research and development to enhance their economic viability and environmental sustainability, as reported in review articles (Zhang *et al*., 2020; White *et al*., 2021).

Therefore, the design of compressors with optimized aerodynamic and structural efficiency assumes critical significance. Excessive vibrations resulting from operations within resonance regions pose a substantial concern in turbomachinery design due to their potential to induce fatigue failures (Zhang *et al*., 2016). To achieve a more efficient

and failure-resistant machine, this study proposes the implementation of a structural optimization process specifically tailored for integrated bladed disks (blisks) as used in centrifugal compressors. The primary focus of this process is to minimize the risk of resonance occurrence.

2. OPTIMIZATION PROCESS

This study introduces a structural design optimization process for blisks, specifically focusing on an sCO2 centrifugal compressor used in a Carbon Capture, Storage, and Utilization (CCSU) project. The identical optimization strategy used in prior studies (Hecker *et al*., 2011; Hinkle, 2016; Martin *et al*., 2019) was employed, leveraging a surrogate-based optimization technique. Throughout this text, the terms 'surrogate model' and 'metamodel' will be used interchangeably. Computational tools such as Ansys® Mechanical and MATLAB® were applied for simulations, calculations, and post-processing.

The optimization procedure, as illustrated in Figure 1, aims to ensure structural integrity by considering safety factors and mitigating the risk of resonance. The vibration analysis considers rotational effects, which are often overlooked in conventional modal analysis and structural optimization. These rotational effects include centrifugal stiffening, spin softening, and Coriolis/Gyroscopic effects (Ruffini *et al*., 2015; Ruffini *et al*., 2017).

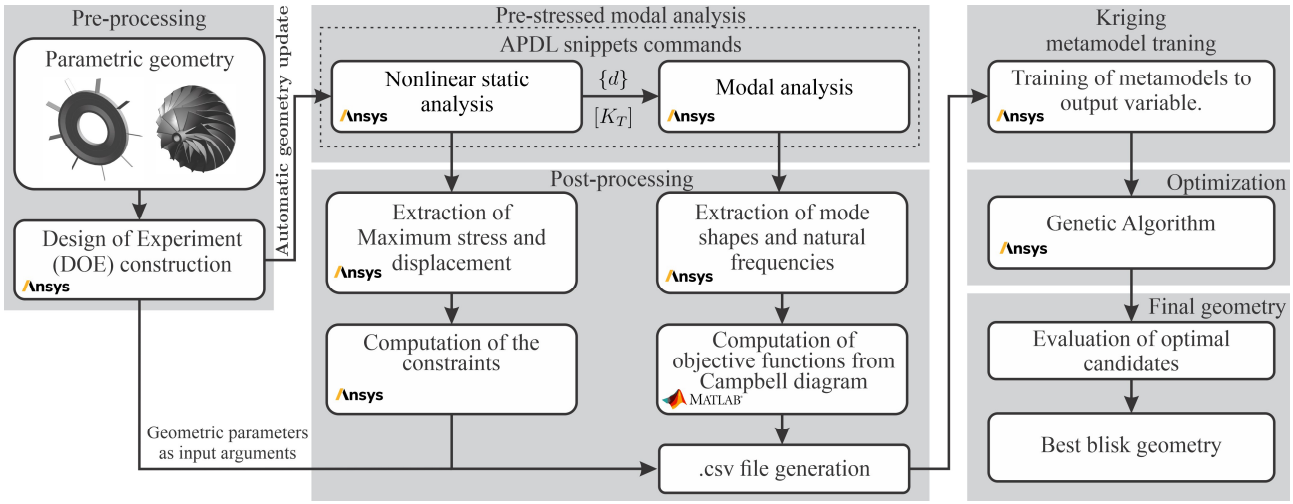

Figure 1 - Optimization process.

2.1 Pre-processing

As illustrated in Figure 1, the process begins with the parametrization of the geometry, followed by the generation of a computational Design of Experiment (DoE). The DoE includes input and output parameters that form the training database for the metamodel. It was created using the Latin Hypercube Sampling method (LHS) (Sobester *et al*., 2008), with the assistance of Ansys® DesignXplorer (Ansys, 2021b). LHS ensures that each interval is represented by a single sample point, dividing the parameter space into equal intervals along each dimension. This minimizes sampling error, guarantees full coverage of the design space without duplication, and reduces sample correlation. Consequently, it results in more accurate estimations and requires fewer sample points compared to other methods.

In this study, two distinct integrated bladed disk (blisk) geometries were employed as models for the case studies. The first model represents a simplified example of an axial compressor/turbine. This choice was made because the objective functions (OF) had previously been applied exclusively to axial-flow turbomachinery (Hecker *et al*., 2011; Hinkle, 2016; Martin *et al*., 2019). The second model considered is an impeller from a sCO2 centrifugal compressor. Detailed representations of the geometries, finite element meshes, and parameterization for both cases can be found in Figure 2 and in Figure 3. The geometries were designed with cyclic symmetry to reduce model complexity, as depicted in Figure 2b and in Figure 3b, where only the sectors were discretized using quadratic tetrahedron elements.

It was assumed that the entire blisk in the first model was fabricated using standard structural steel with a yield strength (σ_Y) of 250 MPa, an ultimate strength (σ_U) of 460 MPa, and a Young's modulus of 200 GPa. In the second case, the material selected for the centrifugal compressor was the alloy 13Cr-4Ni (UNS S42400), based on the material properties outlined in (Dowson *et al*., 2008). This material exhibits a yield strength (σ_Y) of 552 MPa, an ultimate strength (σ_U) of 689 MPa, and a Young's modulus of 220 GPa.

Figure 2c provides a detailed overview of the parameters used to parameterize the sector geometry of the axial blisk. The baseline values for each parameter are listed in Table 1, and the parameterization process is referenced from the work of Armand (1995). In the case of the centrifugal compressor's geometry, only the disk profile was parameterized to prevent

any adverse effects on aerodynamic performance, precisely, seven parameters were employed to describe the disk geometry, as shown in Figure 3c, including the fillet between the hub and blades. This modification was necessary to preserve aerodynamic performance. Specific values of the parameters are subject to a non-disclosure agreement with our project partners.

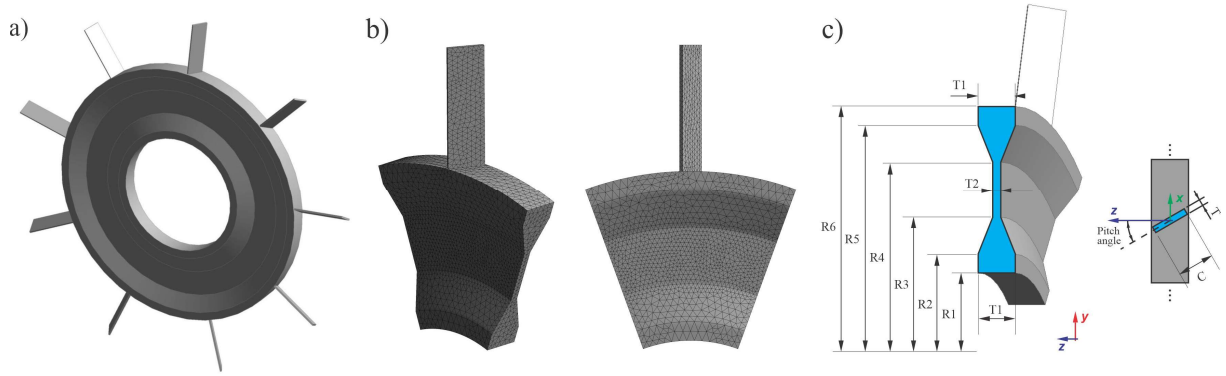

Figure 2 - Axial compressor computational model: a) 3D geometry; b) FE mesh; c) Parameters.

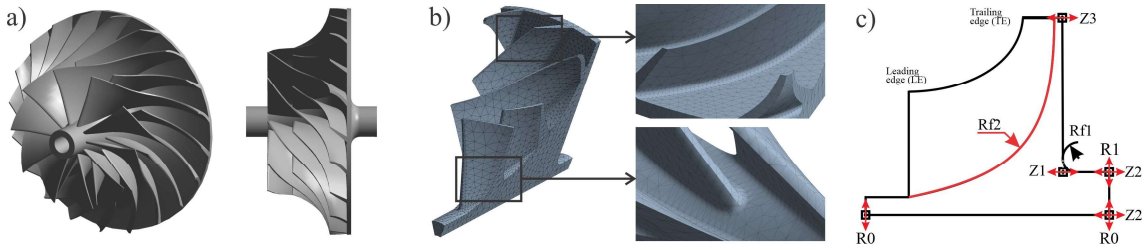

Figure 3 - Centrifugal compressor computational model: a) 3D geometry; b) FE mesh; c) Parameters.

Table 1 - Parameters values of the axial blisk geometry model.

L [mm]	T [mm]	C [mm]	Pitch [°]	R1 [mm]	R2 [mm]	R3 [mm]	R4 [mm]	R5 [mm]	R6 [mm]	T1 [mm]	T2 [mm]
100.0	3.0	30.0	30.0	110.0	125.0	155.0	200.0	230.0	245.0	30.0	6.5

2.2 Pre-stressed modal analysis

To address non-linear effects in modal analysis, the pre-stressed modal analysis approach, as depicted in Figure 4 (Ansys, 2021a), is employed. Initially, a non-linear finite element static analysis is conducted iteratively using the Newton-Raphson method. At each sub-step, the global tangent matrix, also known as the stiffness matrix, is computed until the difference between the internal and external loads satisfies a specified convergence criterion (Crisfield *et al.*, 2012). The resulting final equilibrium state is then saved and utilized as the initial condition for the subsequent modal analysis. This approach allows for the incorporation of geometric non-linearities, effectively capturing stress distribution resulting from centrifugal, aerodynamic, and thermal loads, as well as various contact configurations.

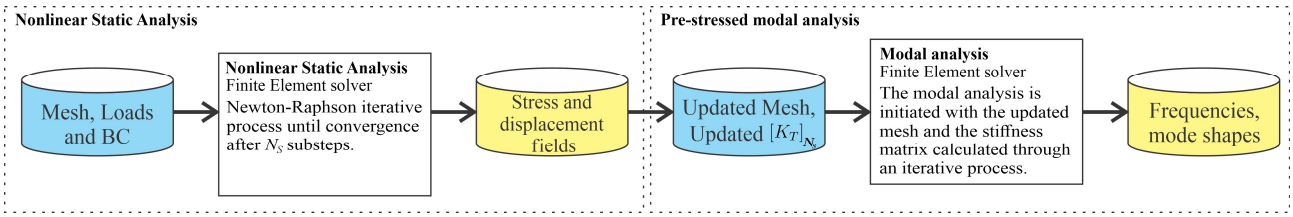

Figure 4 - Pre-stressed modal analysis process.

Simo and Vu-Quoc (1987) demonstrated that an accurate representation of the stiffening effect induced by centrifugal force necessitates the use of a geometrically non-linear theory. Equation 1 represents the non-linear static structural finite element analysis (FEA).

$$([K_M] + [K_G(d,\Omega)] - [K_S(\Omega)])\{\mathrm{d}\} = \{F_C\}, \tag{1}$$

where $[K_M]$ is the elastic stiffness matrix, $[K_G(d,\Omega)]$ is the geometric (non-linear) matrix, $[K_S(\Omega)]$ is the spin softening matrix, $\{\mathrm{d}\}$ is the nodal displacement vector, $\{F_C\}$ is the centrifugal force vector, and Ω is the rotational speed.

Regarding the modal analysis, it commences with the formulation of the equation of motion (EoM). In the case of a rotating flexible structure, which considers the Coriolis effect, Eq. 2 defines the EoM. The derivation of this equation can be found in the work by Ruffini (2016), and a detailed explanation is provided in (Lima, 2022). The additional terms introduced in Eq. 2 encompass the mass matrix $[M]$, the pseudo-damping matrix $[G(\Omega)]$, as well as the acceleration and velocity vectors, represented as $\{\ddot{d}\}$ and $\{\dot{d}\}$, respectively.

$$[M]\{\ddot{\mathrm{d}}\} + [G(\Omega)]\{\dot{\mathrm{d}}\} + ([K_M] + [K_G(d,\Omega)] - [K_S(\Omega)])\{\mathrm{d}\} = \{\mathrm{F}\}. \tag{2}$$

Considering $\{F\} = 0$, and substituting a general solution of the type $\{d\} = \{\Psi_r\}e^{\lambda_r t}$ in Eq. 2, the eigenvalue problem of Eq. 3 is obtained.

$$([M]\lambda_r^2 + [G(\Omega)]\lambda_r + [K_T])\{\Psi_r\} = 0, \tag{3}$$

where $[K_T] = [K_M] + [K_G(d,\Omega)] - [K_S(\Omega)]$, λ_r are the eigenvalues, or natural frequencies, and $\{\Psi_r\}$ are the correspondent eigenvectors, or the mode shapes of any mode r.

2.3 Post-processing

In addition to extracting the natural frequencies and mode shapes, the pre-stressed modal analysis, as depicted in Figure 1, also yields the stress and displacement fields. These fields are crucial for ensuring structural integrity, therefore safety factors based on stress were considered and applied as constraints in the optimization process. Three design criteria were employed to establish these constraints. The first two criteria, SF_y and SF_u, are associated with material yield stress and ultimate tensile strength, respectively, as defined by Eq. 4 and Eq. 5 (Armand, 1995). Here, σ_M represents the maximum von Mises stress.

$$SF_y = \frac{\sigma_Y}{\sigma_M} \geq 1.1, \tag{4}$$

$$SF_u = \frac{\sigma_U}{\sigma_M} \geq 1.5. \tag{5}$$

The third factor is specific to high-speed turbomachinery, known as the burst margin (BM) (Medic *et al.*, 2014) (Morris and Burwood-Smith, 1971), and defined by Eq. 6,

$$BM = \sqrt{\frac{0.85\sigma_U}{\sigma_M}} \geq 1.2. \tag{6}$$

The second branch of the post-processing block, as presented in Figure 1, involves generating the Campbell diagram and computing the objective functions. The Campbell diagram, depicted in Figure 5a, is a valuable tool for identifying potential resonance conditions (Wang *et al.*, 1999). Engine orders (EO), represented by black lines with slopes corresponding to their values, indicate harmonic excitations associated with the number of flow obstacles in the system. Colored lines represent the natural frequencies of the structure. Intersections between engine order lines and mode lines are denoted by black dots on the diagram, signifying potential resonance conditions.

The red region in Figure 5a represents the operational range, encompassing normal operating conditions with the highest excitation levels. If an intersection falls within this range, it suggests the possibility of exciting the structure's natural frequency, which can lead to damaging vibrations, failures, or performance degradation. Consequently, this study focuses exclusively on the operational range.

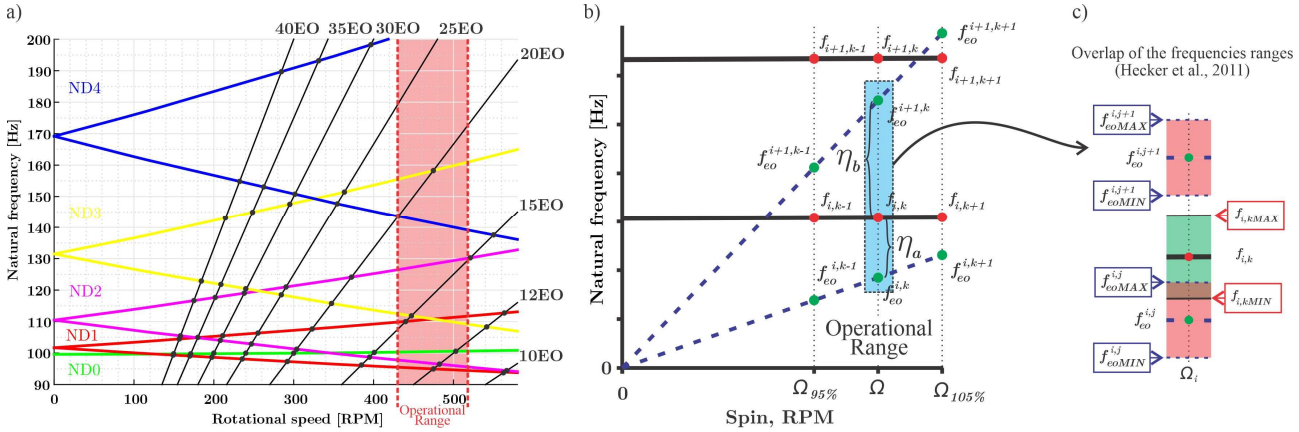

Figure 5 - Resonance identification: a) Campbell diagram example; b) resonance quantification; c) frequencies overlap.

As the primary objective of this study is to mitigate or eliminate the risk of resonance, one possible solution is to eliminate the intersections present in the Campbell diagram. Conventional frequency constraints that focus solely on the first mode or a few low-frequency modes are inadequate for addressing this issue. Therefore, it is crucial to employ methodologies that account for all modes in the Campbell diagram to quantify the resonance risk. In this regard, two objective functions proposed by Hinkle (2016) and Hecker *et al.* (2011) possess this characteristic and will be detailed as follows.

Equation 7 is the quantification of resonance proposed by Hinkle (2016),

$$Z = \sum_{j=1}^{b} \omega_j \eta_j + \sum_{l=1}^{n-b} \omega_l \kappa, \tag{7}$$

where Z is the objective function that must be maximized to obtain a resonance-free structure, b is the number of points considered in resonance, n is the number of natural frequencies calculated within the operational range (n depends on the number of modes calculated, the red dots on the diagram in Figure 5b, and the number of rotational speeds considered, e.g., 0.95Ω, Ω, and 1.05Ω), $\omega_{i,j}$ are weights, κ is a safety margin, and η_i is the relative frequency ratio between the natural frequencies ($f_{i,k}$) and the excitation frequencies ($f_{eo}^{i,k}$), and it is calculated as described by Eq. 8 and illustrated in Figure 5b. The index $i = 1,2,\dots,n$ is referent to the total numbers of modes calculated, and $k = 1,2,3$ is related to the number of rotational speed values used during the simulations.

$$\eta_{i,k} = \frac{\left|f_{eo}^{i,k} - f_{i,k}\right|}{f_{eo}^{i,k}}. \tag{8}$$

Hinkle (2016) established that any natural frequency ($f_{i,k}$) in the Campbell diagram with $\eta_{i,k}$ less than κ is in resonance. To steer the objective function toward a resonance-free design, η is constrained to be equal to κ for the points that are not in resonance. This approach limits the influence of these points on the value of Z and increases the weight of the points that are likely to be in resonance. Consequently, the optimization target is set as $Z_{max} = n\kappa$, implying that all modes are free from resonance.

Additionally, Hecker *et al.* (2011) also quantified the resonance risk by considering the proximity between the natural frequencies and the excitation frequencies. However, unlike Hinkle (2016), Hecker *et al.* (2011) did not use exact values but instead employed frequency ranges, as illustrated in Figure 5c. The ranges of frequencies (Eq. 9 and Eq. 10) are defined by two parameters d_1 and d_2 , as follows,

$$\begin{aligned} f_{eoMIN}^{i,k} &= (1 - d_1)EO\Omega; \\ f_{eoMAX}^{i,k} &= (1 + d_1)EO\Omega; \end{aligned} \tag{9}$$

$$\begin{aligned} f_{MIN,i,k} &= (1 - d_2)EO\Omega; \\ f_{MAX,i,k} &= (1 + d_2)EO\Omega. \end{aligned} \tag{10}$$

Where EO is the engine order value.

Based on these ranges, Hecker *et al.* (2011) established Eq. 11 as an objective function to quantify resonance.

$$P = \sum_{k=1}^{3} P_{\Omega}^{k} \left(\sum_{i=1}^{n} P_F^{i,k} P_{EO}^{i,k} P_M^{i,k} \right), \tag{11}$$

where P_{Ω}^{k} represents the penalty factor for rotational speed, while $P_{EO}^{i,k}$ denotes the penalty factor for each type of engine order. For instance, a crossing between an engine order $EO = 1$ and any natural frequency is considered the most critical situation, as 1EO represents the excitation frequency of the engine. $P_{M}^{i,k}$ serves as the penalty factor related to the type of mode shape, and $P_{F}^{i,k}$ is defined as the penalty factor based on the overlap of the excitation and natural frequencies, as illustrated in Figure 5c, in which the overlap is represented by the intersection between the green and red areas, and is quantified as follows,

$$P_{F}^{i,k} = \min\left(f_{MAX,i,k}, f_{eoMAX}^{i,k}\right) - \max\left(f_{MIN,i,k}, f_{eoMIN}^{i,k}\right). \tag{12}$$

Thus, according to Hecker *et al.* (2011), the smaller the value of the objective function P (Eq. 11), the lower the risk of resonance.

2.4 Metamodel

Metamodel-based optimization is a methodology used to optimize complex systems by employing surrogate models, commonly referred to as metamodels. The central concept behind this approach is to create a surrogate model that accurately approximates the behavior of high-cost functions, such as pre-stressed modal calculations, during the optimization process. This is achieved by constructing the metamodel using a dataset comprising inputs and corresponding outputs obtained from simulations or experiments. In this study, the input parameters consisted of the geometric parameters of the models, while the outputs were determined based on constraints and objective functions derived from post-processing the simulations. Once the metamodel is constructed, it can effectively guide the optimization process.

The Kriging metamodeling technique will be employed as the surrogate model for the output variables (Kianifar and Campean, 2019). A detailed mathematical description of this method can be found in (Sobester *et al*., 2008). To assess the performance of the metamodel, the Design of Experiment (DoE) is divided into two sets: the training dataset and the verification dataset, in a ratio of 80% and 20%, respectively. Four quality criteria are applied, including the coefficient of determination (R^2) greater than 0.9, the root mean square error (RMSE), the maximum absolute error (MAE), and the maximum relative error (MRE), as presented in Eq. 13-15.

$$RMSE = \frac{\sqrt{\frac{1}{n}\sum_{i=1}^{n}(y-\hat{y})^2}}{|\max(y)-\min(y)|} < 5\%, \tag{13}$$

$$MAE = \frac{\max(|y-\hat{y}|)}{|\max(y)-\min(y)|} < 10\%, \tag{14}$$

$$RMSE = max\left(\frac{|y-\hat{y}|}{y}\right) < 5\%. \tag{15}$$

Where y are the observed values of the variables obtained by the simulations and $\hat{y}$ are the predicted values by the Kriging method.

2.5 Optimization statement

The optimization phase, as depicted in Figure 1, is a critical step preceding the evaluation of the new geometry. Given the high-dimensional nature of the problem, which arises from numerous geometric parameters, constraints, and objective functions, we selected a genetic algorithm optimization strategy. In this work, we employed the MOGA (multi-objective genetic algorithm) provided by Ansys® DesignXplorer (Murata *et al*., 1995).

As mentioned previously, two different objective functions, proposed by Hinkle (2016) and Hecker *et al*. (2011), were utilized to quantify the resonance risk. To address this, we implemented two optimization strategies, as described by Equations 16 and 17. These strategies correspond to the specific objective functions and aim to minimize the resonance risk in the design process.

Hinkle: find the geometric parameters which maximize Z.
subject to $SF_y \geq 1.1$,
$SF_u \geq 1.5$,
$BM \geq 1.2$,
$DispMax \leq DispMax_0$,
$Mass \leq Mass_0$. (16)

Hecker: find the geometric parameters which minimize P.

$$\text{subject to } SF_y \geq 1.1, \quad SF_u \geq 1.5, \quad BM \geq 1.2, \quad DispMax \leq DispMax_0, \quad Mass \leq Mass_0. \tag{17}$$

Where the subscript in terms $DispMax_0$ and $Mass_0$ refers to the values of the baseline case used as reference.

3. OPTIMIZATION CASE STUDIES

As previously discussed, this work focuses on two blisks, leading to the implementation of two case studies to assess the proposed optimization strategies for mitigating resonance risk. The first case study involves a simplified axial compressor geometry, while the second centers on the sCO2 centrifugal compressor.

3.1 Axial compressor blisk

When applying the optimization process to the axial compressor case, we obtained the geometries presented in Figure 6b and in Figure 6c for the Hecker and Hinkle strategies, respectively (Figure 6a represents the baseline).

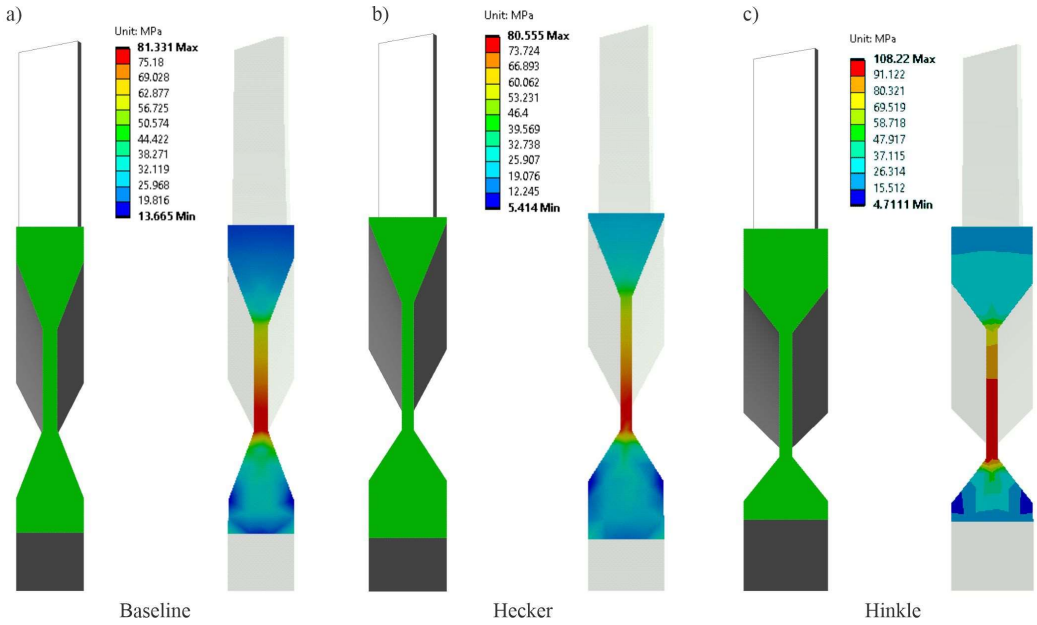

Figure 6 - Axial compressor blisk: a) Baseline geometry and stress results; b) Hecker geometry and stress results; c) Hinkle geometry and stress results.

The results of the static stress analysis are shown in Figure 6a, Figure 6b, and Figure 6c. When consolidating all the static stress data in Table 2, it becomes evident that the geometry optimized using Hecker's strategy outperforms both the baseline and Hinkle's strategy. The optimized design exhibits a significant 13% reduction in mass, a 7% decrease in maximum displacement, and a 1% decrease in stress levels. These improvements have led to an overall increase in all safety factors.

Table 2 - Summary of static stress analysis for the axial compressor case.

Opt. Strategy	$Mass$ [kg]	$DispMax$ [mm]	σ_M [MPa]	SF_Y	SF_U	BM
Baseline	21.7 (-)	0.0513 (-)	81.3 (-)	3.07 (-)	5.53 (-)	2.17 (-)
Hecker	18.9 (-13%)	0.0478 (-7%)	80.6 (-1%)	3.10 (0.96%)	5.59 (0.96%)	2.18 (0.48%)
Hinkle	18.9 (-13%)	0.0509 (-1%)	108.2 (33%)	2.31 (-25%)	4.16 (-25%)	1.88 (-13%)

To assess the capability of reducing the risk of resonance through the optimization strategies employed, we present the Campbell diagrams for the baseline design, Hecker's strategy, and Hinkle's strategy in Figure 7a, Figure 7b, and Figure 7c, respectively, for comparison. The baseline geometry displayed four intersection points between the modes (solid black

lines) and the engine order lines (dashed blue lines). The same number of crossing points was observed with the optimized geometry using Hinkle's strategy. However, upon examining the Campbell diagram resulting from the analysis of the optimized geometry using Hecker's objective function (Figure 7b), it's evident that all potential resonance conditions were effectively eliminated. This outcome underscores the effectiveness of Hecker's objective function in mitigating the risk of resonance, thereby ensuring the structural integrity of the axial compressor blisk under the considered analysis conditions.

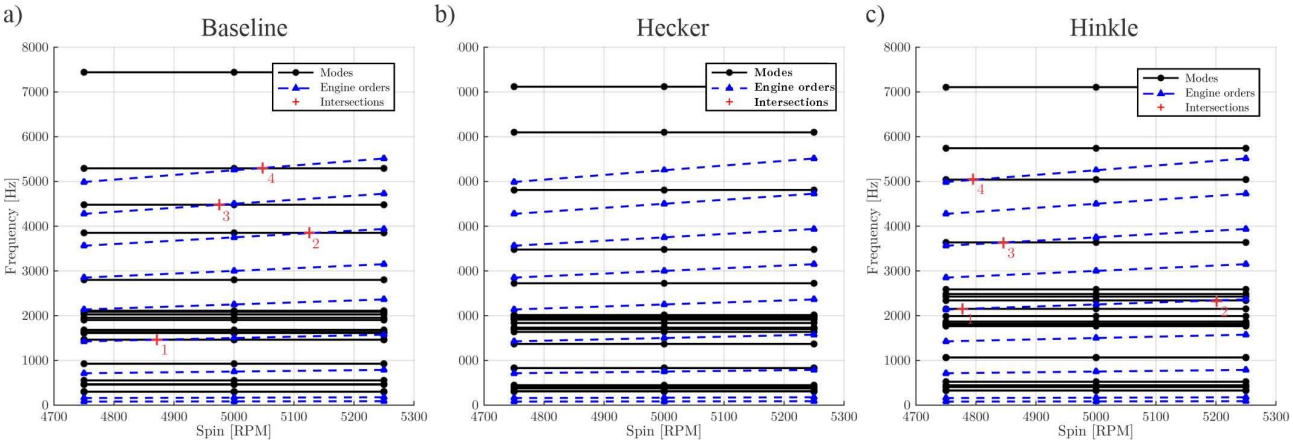

Figure 7 – Campbell diagrams of axial compressor blisk: a) Baseline, b) Hecker strategy; c) Hinkle strategy.

3.2 Centrifugal compressor blisk

Based on the analysis of the first case study, it became evident that Hecker's strategy successfully reduced the resonance risk by eliminating all crossing points on the Campbell diagram. Therefore, for the second case study, only Hecker's optimization strategy was considered. The results of the modal analysis conducted on the baseline and optimized geometries are presented in Figure 8, where Figure 8a represents the baseline, and Figure 8b illustrates the new geometry obtained through optimization. The number of crossing points was reduced from six to four, thus lowering the risk of resonance. A closer examination of the low-frequency regions highlighted in Figure 8c and Figure 8d reveals that the intersection with the first mode has been eliminated. Although the optimized geometry did not eliminate all crossing points, it effectively mitigated the risk of resonance.

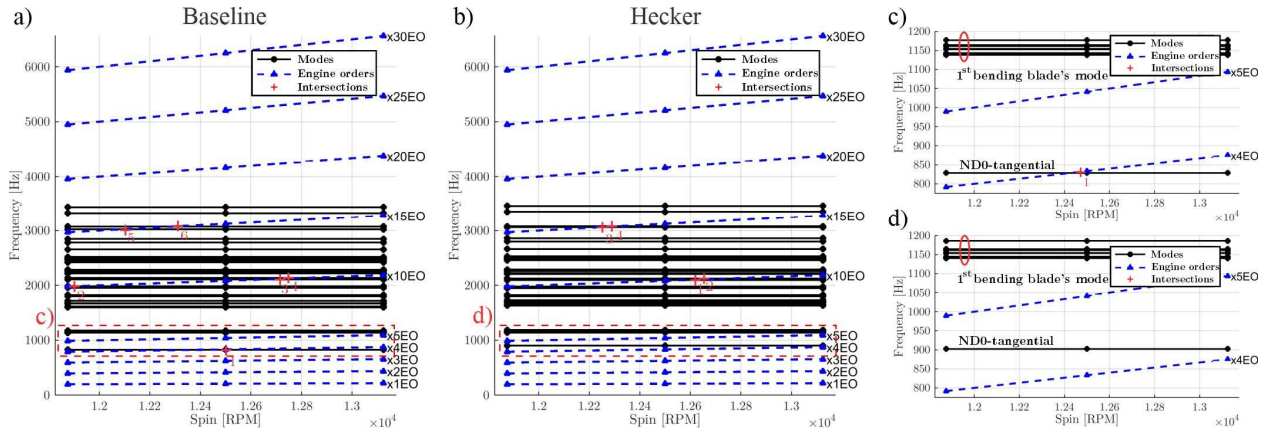

Figure 8 - Campbell diagrams of centrifugal compressor blisk: a) Baseline, b) Hecker strategy; c) Low-frequency region of baseline; d) Low-frequency region of optimized geometry by Hecker's strategy.

In the static stress analysis, the results were compiled and listed in Table 3. When examining the results for the baseline geometry, it became apparent that it did not meet the design criteria for SF_u and BM (Equations 5 and 6). However, through optimization, the stress levels were reduced by 16.4%, resulting in significant increases in the safety factors SF_y, SF_u, and BM by 19.6%, 19.6%, and 9.35%, respectively. This improvement ensures the static structural integrity of the centrifugal compressor. Despite the reduction in stress levels, the mass of the optimized geometry remained unchanged compared to the baseline case, thus preserving performance. Another critical consideration for open

impellers is the gap clearance, influenced by blade deformation under load. Consequently, the 15.5% reduction in maximum displacements also signifies an enhancement in compressor performance.

Table 3 - Summary of static stress analysis for the centrifugal compressor case.

Opt. Strategy	$Mass$ [kg]	$DispMax$ [mm]	σ_M [MPa]	SF_y	SF_u	BM
Baseline	8.10 (-)	0.61 (-)	469 (-)	1.18 (-)	1.47 (-)	1.118 (-)
Hecker	8.09 (-0.21%)	0.51 (-15.5%)	392 (-16.4%)	1.41 (19.6%)	1.76 (19.6%)	1.22 (9.35%)

Figure 9 visually represents the static stress analysis of the baseline and optimized geometries for the centrifugal blisk. In both geometries, the maximum displacement was located at the tip of the main blades (Figure 9a and Figure 9d). However, regarding the location of the maximum stress (Figure 9b and Figure 9e), it shifted from the root of the main blade to the mid-span of the trailing edge of the splitter blade in the optimized geometry, resulting in the previously mentioned 16.4% reduction.

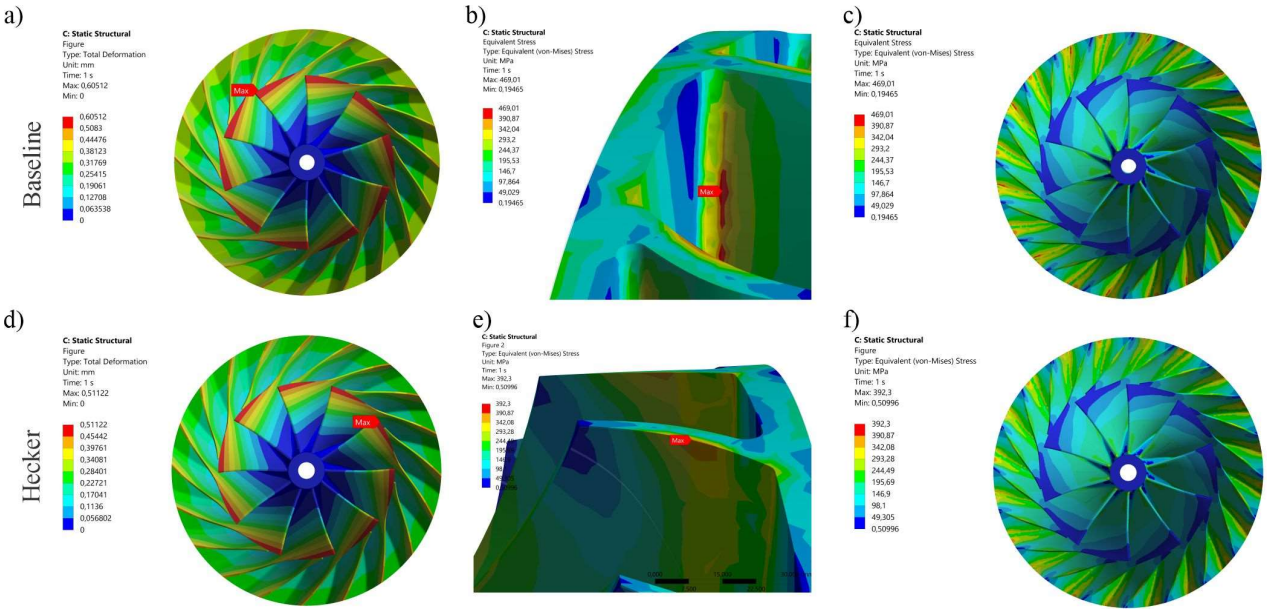

Figure 9 - Centrifugal compressor blisk: a) baseline: displacement field; b) baseline: maximum stress; c) baseline: stress field; d) optimized: displacement field; e) optimized: maximum stress; f) optimized: stress field.

4. CONCLUSION

In conclusion, this study focused on optimizing axial and centrifugal compressor blisks for applications in Carbon Capture, Storage, and Utilization (CCSU) plants. The design of compressors with optimized aerodynamic and structural efficiency is essential to ensure their reliability and performance. Resonance-induced vibrations pose a significant challenge in turbomachinery design, necessitating effective strategies to mitigate this risk.

Metamodel-based optimization, utilizing the Kriging metamodeling technique, was employed to optimize the geometry of the blisks and avoid resonance conditions. The results demonstrated the efficacy of the optimization strategies in reducing resonance risk and enhancing structural integrity for both case studies.

The axial compressor blisk case study revealed that Hecker's objective function outperformed both the baseline and Hinkle's strategy. The analysis of Campbell diagrams confirmed the successful elimination of resonance conditions with Hecker's strategy. Although not all crossing points were eliminated in the centrifugal compressor blisk case study, a significant reduction in the risk of resonance was achieved. Additionally, the static stress analysis demonstrated a decrease in stress levels while maintaining the baseline case's mass, thus ensuring the static structural integrity.

In summary, this study successfully demonstrated the effectiveness of the proposed optimization strategies in reducing resonance risk and enhancing the structural integrity of centrifugal compressor blisks. These findings contribute to the development of efficient and reliable turbomachinery designs for sCO2 applications in CCSU. Future research can focus on exploring additional optimization strategies and considering the impact of aerodynamic loads to further enhance the robustness of the designs.

5. ACKNOWLEDGEMENTS

We gratefully acknowledge the support of the RCGI – Research Centre for Greenhouse Gas Innovation, hosted by the University of São Paulo (USP) and sponsored by FAPESP – São Paulo Research Foundation (2014/50279-4 and 2020/15230-5) and Shell Brazil, and the strategic importance of the support given by ANP (Brazil's National Oil, Natural Gas, and Biofuels Agency) through the R&D levy regulation. Also, the support of the UFABC – Federal University of ABC, which provides all the computational and physical infrastructure.

6. REFERENCES

Ansys, 2021a. "Ansys mechanical apdl theory reference". Canonsburg, PA, USA: ANSYS Inc.

Ansys, 2021b. "Designxplorer user's guide. canonsburg". Canonsburg, PA, USA: ANSYS Inc.

Armand, S. C., 1995. "Structural optimization methodology for rotating disks of aircraft engines". NASA Technical Memorandum (No. NASA-TM-4693).

Baena-Moreno, *et al*., 2019. "Carbon capture and utilization technologies: a literature review and recent advances". Energy Sources, Part A: Recovery, Utilization, and Environmental Effects, 41(12), 1403-1433.

Bui, M., *et al*., 2018. "Carbon capture and storage (CCS): the way forward". Energy & Environmental Science, 11(5), 1062-1176.

Crisfield, M. A., *et al*., 2012. "Nonlinear finite element analysis of solids and structures". John Wiley & Sons.

Dowson, P., Bauer, D., & Laney, S., 2008. "Selection of materials and material related processes for centrifugal compressors and steam turbines in the oil and petrochemical industry". In Proceedings of the 37th turbomachinery symposium. Texas A&M University. Turbomachinery Laboratories.

Hecker, P., *et al*., 2011. "Process integration and automated numerical design optimization of an eigenfrequency analysis of a compressor blade". In Turbo Expo: Power for Land, Sea, and Air (Vol. 54662, pp. 791-800).

Hinkle, K. B., 2016. "An automated method for optimizing compressor blade tuning". Master's thesis, Brigham Young University.

Kianifar, M. R., & Campean, F., 2020. "Performance evaluation of metamodelling methods for engineering problems: towards a practitioner guide". Structural and Multidisciplinary Optimization, 61(1), 159-186.

Lima, D. Z., 2022. "Análise modal e otimização de rotores de pás integradas com aplicação em compressores centrífugos para CO2 supercrítico (in English)". Master's thesis, Graduate Program in Mechanical Engineering, Federal University of ABC, Santo André, Brasil.

Medic, G., *et al*., 2014. "High efficiency centrifugal compressor for rotorcraft applications". (No. NASA/CR-2014-218114).

Morris, A. W. H., & Burwood-Smith, A., 1971. "High Temperature Turbines". AGARD-CP-73-71.

Murata, T., *et al.*, 1995. "MOGA: multiobjective genetic algorithms". In: IEEE international conference on evolutionary computation, IEEE Piscataway, NJ, USA, vol 1, pp 289–294.

Ruffini, V., Schwingshackl, C., & Green, J., 2015. "Experimental and analytical study of Coriolis effects in bladed disk". In International Design Engineering Technical Conferences and Computers and Information in Engineering Conference (Vol. 57181, p. V008T13A070). American Society of Mechanical Engineers.

Ruffini, V., 2016. "Coriolis effects in bladed discs". PhD thesis, Imperial College London.

Ruffini, V., Green, J. S., & Schwingshackl, C. W., 2017. "The influence of mistuning and coriolis effects on the modal parameters of bladed discs: An experimental study". In Turbo Expo: Power for Land, Sea, and Air (Vol. 50930, p. V07BT35A006). American Society of Mechanical Engineers.

Simo, J. C., & Vu-Quoc, L., 1987. "The role of non-linear theories in transient dynamic analysis of flexible structures". Journal of Sound and Vibration, 119(3), 487-508.

Sobester, A., Forrester, A., & Keane, A., 2008. "Engineering design via surrogate modelling: a practical guide". John Wiley & Sons.

Wang, Q., Bartos, J. C., & Houston, R. A., 1999. "Methodology Of Open Bladed Impeller Resonance Indentification". In Proceedings of the 28th Turbomachinery Symposium. Texas A&M University. Turbomachinery Laboratories.

White, M. T., *et al*., 2021. "Review of supercritical CO2 technologies and systems for power generation". Applied Thermal Engineering, v. 185, p. 116447, 2021.

Zhang, M., Liu, Y., Wang, W., Wang, P., & Li, J., 2016. "The fatigue of impellers and blades". Engineering Failure Analysis, 62, 208-231.

Zhang, Z., *et al*., 2020. "Recent advances in carbon dioxide utilization". Renewable and sustainable energy reviews, v. 125, p. 109799.

7. RESPONSIBILITY NOTICE

The authors are the only responsible for the printed material included in this paper.